Journal of Applied Fluid Mechanics, Vol. 17, No. 4, pp. 870-888, 2024.
Available online at www.jafmonline.net, ISSN 1735-3572, EISSN 1735-3645.
https://doi.org/10.47176/jafm.17.4.2204

Study on the Effect of Bridge Windbreaks on the Aerodynamic Characteristics of High-Speed Trains Meeting under Crosswind

L. X. Chen, A. F. Jin† and X. C. Jia

College of Mechanical Engineering, Xinjiang University, Urumqi 830047, China

†*Corresponding Author Email: jinaf3500_xju@xju.edu.cn*

ABSTRACT

Under the influence of crosswind, when high-speed trains (HSTs) meet on a bridge, they produce complex vortexes, strong aerodynamic loads, and other aerodynamic effects. The purpose of this paper is to reveal the influences of crosswind and windbreaks on the vortexes generated by HSTs, the pressure distributions on the surfaces of the trains, and the aerodynamic load coefficients of the trains when they meet on a bridge, as well as the influence of the pressure waves generated by the trains on the windbreaks. The three-dimensional incompressible improved delayed detached eddy simulation (IDDES) method based on the SST k-ω turbulence model is used for numerical calculation purposes, and the overset grid method is used to realize the relative motions of the trains. The results show that the windbreaks can reduce the negative pressure (NP) imposed on the train surface and effectively improve the pressure distribution; crosswinds have a significant impact on the vortexes generated by trains, and the vortexes generated by the upstream train affect the stability of the downstream train; windbreaks can reduce the aerodynamic load applied when trains meet and thus improve the safety of the trains; and the head and tail waves generated by trains impose pressure on the windbreaks, which affects the reliability of the windbreaks installations. The simulation results can provide a preliminary reference for future research.

Article History

Received August 11, 2023
Revised November 21, 2023
Accepted November 23, 2023
Available online January 30, 2024

Keywords:

Aerodynamic loading
Bridge
IDDES
Pressure distribution
Vortex

1. INTRODUCTION

HSTs have become one of the major modes of transportation for people's daily travels, and their driving safety issues, especially their driving stability under the effect of crosswind, have become some of the most attractive issues in the field of HST aerodynamics (Zhang et al., 2019). The Lanzhou-Xinjiang High-Speed Railway in China has many bridge structures along its whole line. Under the combined action of crosswind and train winds, the aerodynamic performance of trains further deteriorates, which has a negative impact on train safety. This adverse effect is further aggravated when trains meet under crosswind.

Currently, research on what occurs when HSTs meet mainly focuses on the pressure wave generated during the train meeting and the aerodynamic load (Li et al., 2021). Among them, Qiao et al. (2016) studied train meetings under different line spacings between typical HSTs, analyzed the relationship between the line spacings on the pressure wave generated by passing trains according to measured and simulated data, and concluded that the passing pressure wave has an approximately negative exponential relationship with the line spacings. Xi et al. (2016) corrected Steinheur's empirical formula and provided a new formula for calculating the amplitude of the surface pressure wave generated by trains meeting at an equal speed. Li et al. (2015) investigated the aerodynamic characteristics of trains meeting on bridges under the effect of crosswind and showed that the overall pressure distribution on the surface of a train body is no longer symmetrical under the effect of crosswind. Liu et al. (2016) analyzed the transient pressure imposed on the surfaces of trains and the aerodynamic forces and moments on train bodies when 8 trains set at 250 km/h in the 20 m/s crosswind and showed that the pressure difference between the measurement points at the head and the rear of a train during the meeting of a train set in crosswind is large; additionally, the pressure difference between the measurement points at the middle of the train located on the same side is small. Li et al. (2017) studied the aerodynamics of different nose contour shapes of HSTs when they meet in the tunnel. The results show that

NOMENCLATURE

CFD	Computational Fluid Dynamics	NP	Negative Pressure
C_{mx}	overturning moment coefficient	PP	Positive Pressure
C_y	side force coefficient	Q	volumetric flow rate
C_Z	lift coefficient	SIMPLE	Semi-Implicit Method for Pressure Linked Equations
DDES	Delayed Detached Eddy Simulation	SST	Shear Stress Transport
HC	Head Car	TA	Train A
HST	High-Speed Train	TB	Train B
IDDES	Improved Delayed Detached Eddy Simulation	TC	Tail Car
k	turbulence kinetic energy	TS	Top Surfaces
LS	Leeward Side	ω	specific dissipation rate
MC	Middle Car	WS	Windward Side

the aerodynamic performance of shuttle-shaped and flat-width trains is better when they meet in the tunnel.

The above scholars have mainly studied the meeting of HSTs on bright lines, while the following scholars studied the meeting of HSTs on dark lines. Xu et al. (2016) numerically simulated the pressure waves of rendezvous between trains with equal and unequal speeds in a tunnel and initially provided the fitting relation equation between the absolute value of the peak NP of the variable-speed train and the speed of the train during the rendezvous. Lin et al. (2019) studied nine conditions of HSTs meeting in tunnels, analyzed the effect of pressure waves on the strength of a body structure design, and compared the dynamic pressure wave loads produced with equivalent quasistatic load simulations. Mei et al. (2019) investigated the effects of tunnel length, blockage ratio, and train speed on the pressure characteristics of a tunnel. The results showed that the pressure wave of a tunnel rendezvous is closely related to the reflection and superposition of the compression and expansion waves induced by trains driving into and out of the tunnel, and the pressure wave of the tunnel rendezvous increases with the blockage ratio and train speed.

Extensive research has been conducted to ensure the safety of HSTs travelling under crosswind (Xia et al., 2022). The research results show that the most effective measure for reducing the impact of crosswind on the safety of HST operations is to build windproof facilities along the railroad, among which windbreaks are some of the most important facilities; they are widely used in the 100-mile windy area where the Lanzhou-Xinjiang Railway in China passes through (He, 2017). Niu et al. (2022) systematically investigated the effects of unilateral and bilateral windbreaks on the nonstationary aerodynamic performance of a HST and the flow field characteristics around the train by utilizing an improved computational fluid dynamics method and the slip grid technique. Wang et al. (2022) used their developed experimental wind tunnel platform to analyze the dynamic interactions between windbreaks and the aerodynamic characteristics of moving trains and the wind protection performance of windbreaks with different porosities. Zhang et al. (2019) investigated the aerodynamic characteristics of a HST under the combined effects of different windbreaks and yaw angles using numerical simulations. The results showed that windbreaks provide good protection for trains. Zhang et al. (2017a) optimized the shape of the earth embankment windbreaks along the Lanzhou-Xinjiang Railway. The results show that the heightened earth embankment windbreaks can not only reduce the crosswind speed but also be more suitable for engineering construction.

Through the above analysis, it can be seen that the research conducted by domestic and foreign scholars on HST rendezvous focuses on bright line and dark line rendezvous, but the research on bright line rendezvous usually does not consider the impact of windproof structures on HSTs. Therefore, this study takes HSTs meeting on bridges as the research objects, fully considers influence factors such as windbreaks and side winds, and studies the changing rules of aerodynamic performance factors such as the vortexes around a train, the pressure distribution on the train surface, the aerodynamic load of the train, and the influence of a change in aerodynamic performance on the ability of the train to travel safely.

2. NUMERICAL SIMULATIONS

2.1 Geometric Model and Case Setting

In this paper, HSTs operated by the Lanzhou-Xinjiang High-Speed Railway in China are used as the research objects, and a full-size (scale 1:1) train model with three formations (head, middle, and tail cars) is adopted (Cai et al., 2020; Ji et al., 2022). The low influence of pantographs, door handles, windshields, windshield wipers, lamps, and bogies on the aerodynamic loads of trains (Deng et al., 2021). These structures are neglected in the established HST model (Deng et al., 2020; Yang et al., 2021; Wu et al., 2022), as shown in Fig. 1(a). The full-size length (L), width (W), and height (H) of the train model are 76.4 m, 3.4 m, and 3.5 m, respectively, and the lengths of the head car (HC), middle car (MC), and tail car (TC) are 25.7 m, 25 m, and 25.7 m, respectively. In this paper, the model H is selected as the feature size. Figure 1(b) shows a 32-meter simply supported box girder that is often used in the bridge section of the Chinese high-speed railroad (whose model was often used in previous studies), ignoring the abutment, ballast, and track (Deng et al., 2021); the distance between the bottom of the train and the bridge deck is 0.2 m (Xu et al., 2020), and the spacing of the high-speed railroad line is 5 m (Li et al., 2015). Figure 1(c) shows the perforated windbreaks used in the bridge

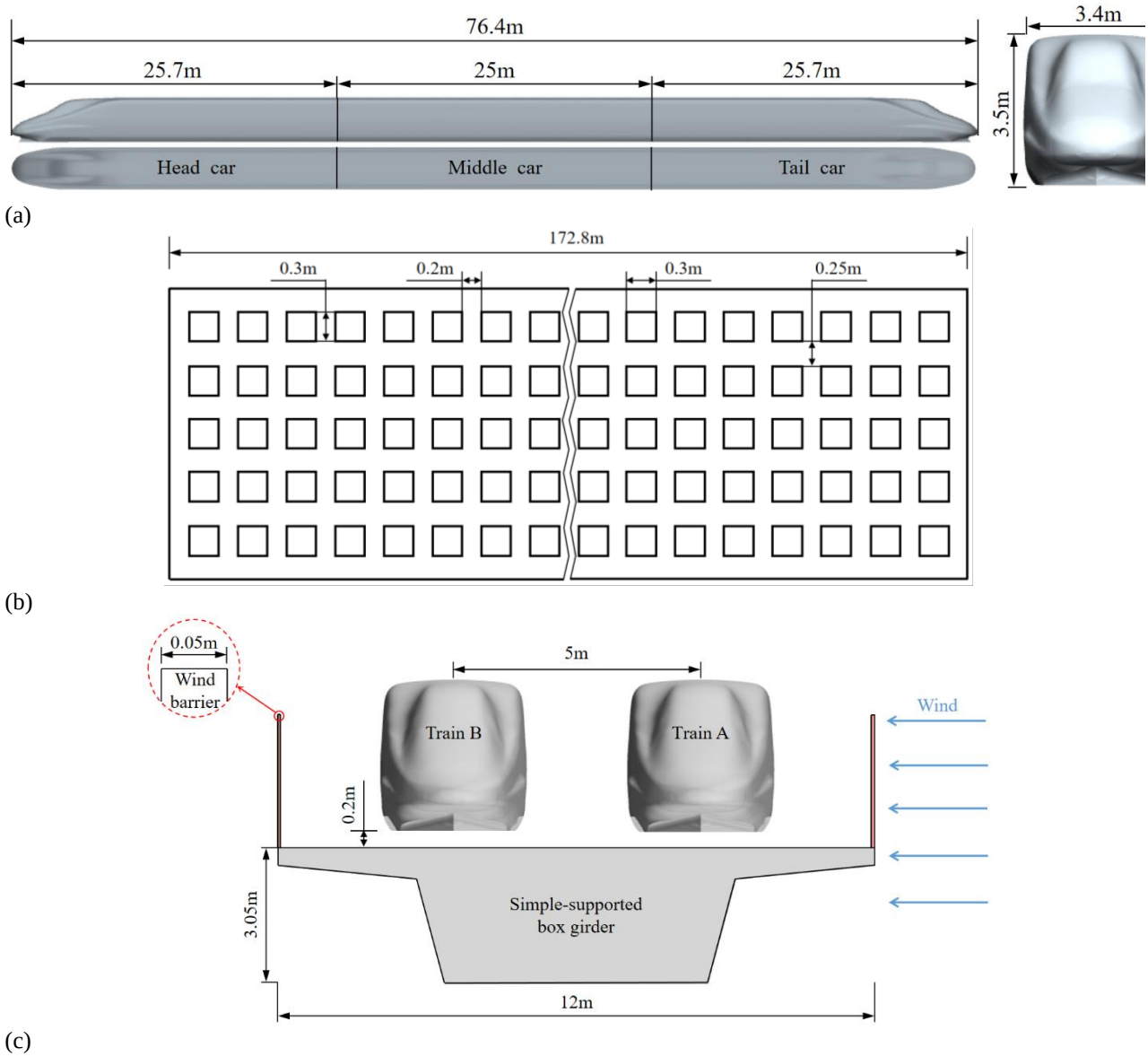

Fig. 1 Calculation model: (a) HST geometry model; (b) Bridge geometry model; (c) Windbreaks geometry model

Table 1 Calculation cases

Cases	Train velocity	Crosswind velocity	Windbreaks
Case 1	70 m/s	0 m/s	×
Case 2	70 m/s	20 m/s	×
Case 3	70 m/s	20 m/s	√

section of the high-speed railroad, which has a height of 3 m, a thickness of 0.05 m, and a porosity of 30%. This model has been used in previous studies (Zhang et al., 2019).

Three computational cases are considered in this study, as shown in Table 1, where Case 1 is the rendezvous of HSTs without the windbreaks and crosswind condition; Case 2 is the rendezvous of HSTs without the windbreaks but with the crosswind condition; and Case 3 is the rendezvous of HSTs with the windbreaks and crosswind condition. By analyzing these three computational cases, specific information can be obtained about the effects of the presence or absence of crosswind and the presence or absence of windbreaks on the aerodynamic performance of trains during HST rendezvous.

2.2 Numerical Method

In this study, the overset grid method is used to simulate the intersection of HST motions. This method has been widely used to study the aerodynamics of HSTs. According to the information released by the State Railway Administration of China, the Lanzhou-Xinjiang high-speed railroad line is designed to operate at a maximum speed of 250 km/h. When a HST runs at 250 km/h, its Mach number is less than 0.3, and its air flow is regarded as incompressible flow (Niu et al., 2022). Therefore, an incompressible turbulence model is used in this study to investigate the aerodynamics of HST rendezvous. In previous studies on the aerodynamics of HSTs, the IDDES method was widely used (Li et al., 2020; Deng et al., 2021; Niu et al., 2022; Yao et al., 2022). The IDDES model was developed by Shur et al. (2008) from the delayed detached eddy simulation (DDES) model. In this study, the IDDES approach based on the SST k-ω

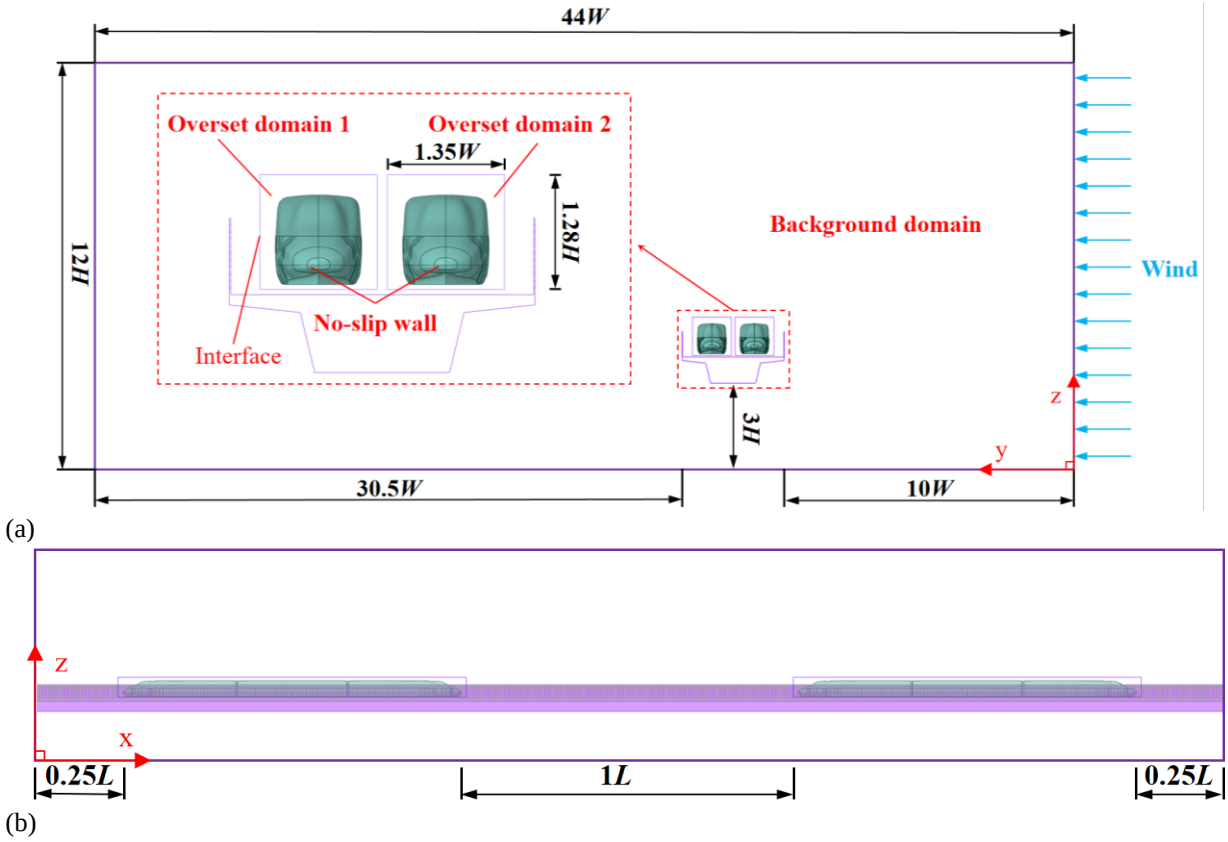

Fig. 2 Computational domain: (a) Front view; (b) Right view

turbulence model is used to simulate the unsteady flow fields and aerodynamic forces of HSTs.

Herein, a standard wall function is used to address the wall effect, which is solved using a finite volume solver that separates incompressible and unstructured. The semi-implicit method for pressure-linked equations (SIMPLE) algorithm has been widely used in HST computations (Liang et al., 2022), so the SIMPLE algorithm with pressure-related equations is used to solve the coupled equations of pressure and velocity. The convection term is switched between the bounded central difference scheme and the second-order upwind scheme using a hybrid scheme (Zhang et al., 2017b; Xu et al., 2019). The time integration process uses an implicit second-order scheme. The entire transient solution time is 2 s, and the time step size is 1×10^ (-3) s. Each time step is iterated 30 times. A time-step independence verification is performed in the third section. This simulation is carried out on a supercomputer service platform.

2.3 Computational Domain and Boundary Condition

In this study, the overset grid method is used to simulate the intersection of HST motions. This method has been widely used in studies on the aerodynamics of HSTs (Meng et al., 2021). The overset grid method divides the entire computational domain into a stationary background region and moving overset regions. In Fig. 2 (a), two purple wireframe regions containing HSTs with heights and widths of 1.28 H and 1.35 W are the overset regions, and the entire region containing the cuboid shape of the bridge and the windbreaks is the background region. The flow field information of the two types of regions interacts through the interface. The grid sizes on the boundaries of the overset regions should be the same as the grid size of the background region, which is more conducive to the interaction of the flow field information.

The computational domain must be selected without affecting the fluid flow in the vicinity of the moving trains, and the computational efficiency should be considered. Because the flow field is not stable at the beginning of the simulation calculation, it is necessary to wait for the flow field to stabilize before the two trains enter the rendezvous phase (Li et al., 2015). Therefore, taking computational efficiency into account, two HSTs are 1 L away from each other. The overall length, width, and height of the computational domain are chosen to be 3.5 L, 44 W, and 12 H, respectively, fully considering the movement of the trains, the strong lateral winds, and the effect of the bridge. As shown in Fig. 2(a), the distance between the bottom of the bridge and the bottom of the fixed domain is 3 H, and the distance between the right side of the bridge and the entrance of the fixed domain is 10 W. As shown in Fig. 2(b), the nose tip of the TC of the two HSTs is 0.25 L away from the left and right boundaries, respectively. The boundary conditions are set as shown in Fig. 2(a) and Fig. 4. 1) The boundary conditions of the two moving domains are defined as overlapping boundary conditions. 2) The left, right, and rear end faces of the fixed domain are defined as the pressure outlet boundary conditions. 3) The top of the fixed domain is defined as a symmetric boundary condition. 4) The velocity inlet boundary condition is defined at the front end of the fixed domain. 5) The bottoms of the fixed domain, bridges, windbreaks, and HST bodies are defined as nonslip wall boundary conditions.

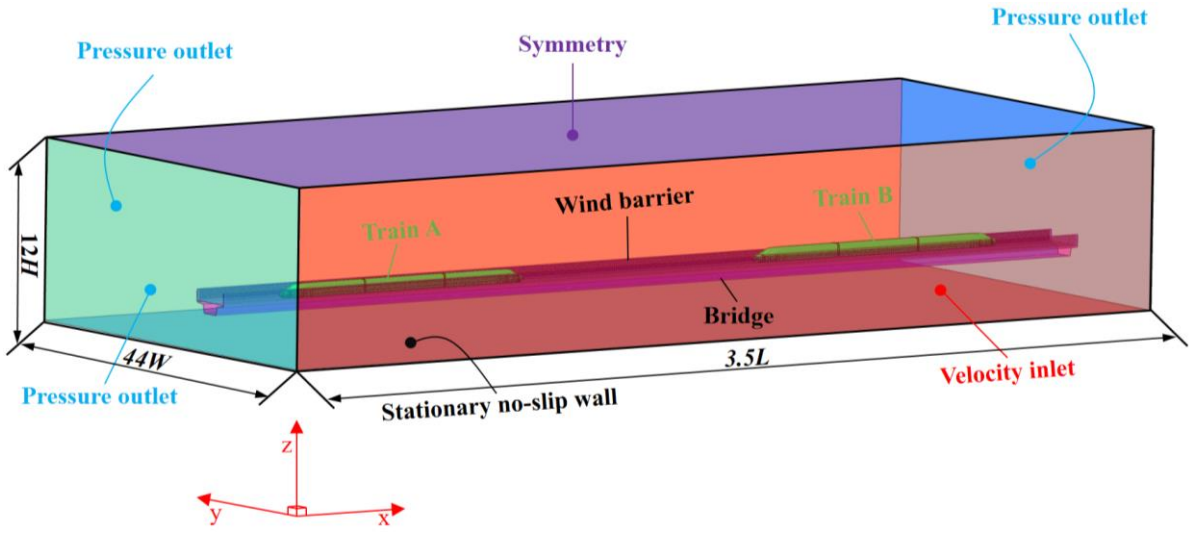

Fig. 3 Boundary conditions

2.4 Aerodynamic Load Calculation

The dimensionless aerodynamic parameters used in this study are the side force coefficient (C_y), lift coefficient (C_z), and overturning moment coefficient (C_{mx}), which are defined as follows:

$$C_y = \frac{F_y}{0.5\rho V_R^2 S_1} \tag{1}$$

$$C_z = \frac{F_z}{0.5\rho V_R^2 S_2} \tag{2}$$

$$C_{mx} = \frac{M_x}{0.5\rho V_R^2 S_2 W} \tag{3}$$

where F_y, F_z, and M_x are the side force, lift force, and overturning moment, respectively, and the train forces are shown in Fig. 4. S_1, S_2 and W are the side area, bottom area, and width of the HST, respectively, and ρ is the air density (1.225 kg/m^3). As shown in Fig. 5, V_R is the synthesized velocity, which is determined by the vectors of the crosswind velocity (U) and the train velocity (V_{tr}), which are defined as follows:

$$V_R = \sqrt{(V_{tr}^2 + U^2)} \tag{4}$$

$$\beta = tan^{-1}\left(\frac{U}{V_{tr}}\right) \tag{5}$$

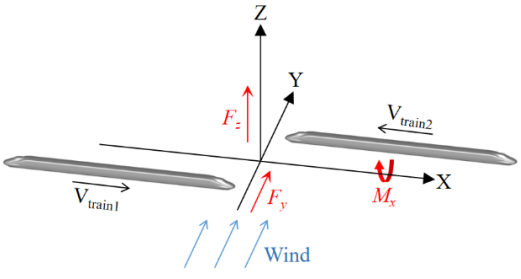

Fig. 4 Aerodynamic and torque diagram of the trains

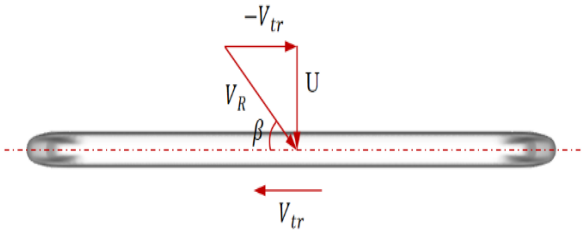

Fig. 5 Composite wind speed diagram

2.5 Grid Generation

When using computational fluid dynamics (CFD) for numerical simulation purposes, obtaining reasonable and high-quality grids can improve the accuracy and efficiency of the calculation process. The overset grid method used in this study needs to divide the computational domain into a background domain and two overset domains. The overset domains contain HSTs with complex shapes, while the background domain contains bridges and perforated windbreaks. The computational domain grid is shown in Fig. 6. To obtain more accurate aerodynamic loads for the HSTs and capture the vortexes around the trains and the windbreaks, the grid is encrypted around the trains and the downstream areas of the windbreaks, the grid is encrypted around the trains and the downstream areas of the windbreaks. To more accurately capture the velocity and pressure changes on the boundary, a boundary layer must be set up on the surface of each train as well as on the surface of each windbreak. The boundary layer height around the windbreak is 30 mm, the number of layers is 10, and the growth rate is 1.3; the boundary layer height around the HSTs is 50 mm, the number of layers is 15, and the growth rate is 1.3. The entire computational domain has 49 million grids. Considering that the speed of each HST in this study is 70 m/s, the crosswind velocity is 20 m/s, the height of each train is 3.5 m, and the Reynolds number of the simulation is approximately 1.68×10^7.

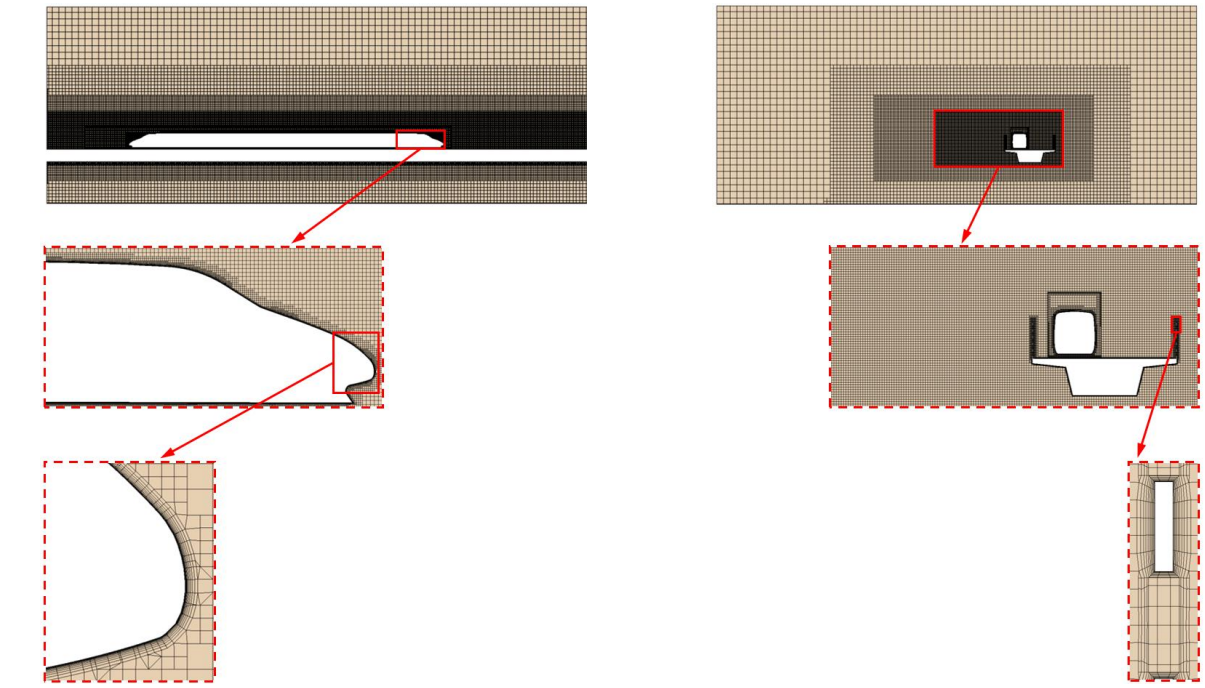

(a) (b)

Fig. 6 (a) Grid around a train; (b) Grid around a windbreak

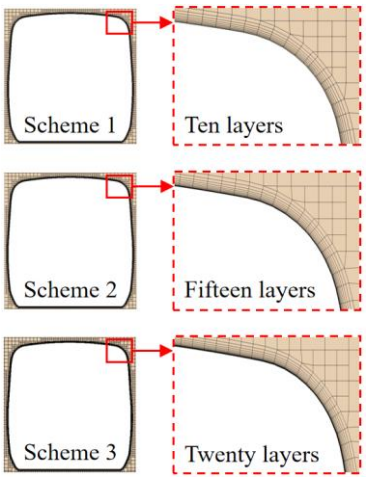

Fig. 7 Boundary layer grids of different schemes

3. COMPUTATIONAL VALIDATION

3.1 Grid Independence Verification

The number of layers in the boundary layer around a train directly affects the calculation accuracy of the flow field around the train and the required computing resources (Ouyang et al., 2023). Therefore, in the case in which the y+ value of the first boundary layer needed by the turbulence model is satisfied, by changing the number of boundary layers around the train, a grid generation scheme that satisfies the required calculation accuracy and saves computing resources is found. As shown in Fig. 7, three schemes are used, and they have ten, fifteen, and twenty boundary layers. Under the condition of Case 3, the grids of these three schemes are simulated and calculated, and the optimal scheme is selected by comparing the C_y of the HC of train A (TA) and the C_y of the HC of train B (TB). The numbers of grids used for Scheme 1, Scheme 2, and Scheme 3 are 43 million, 49 million, and 55 million, respectively. From Figs. 8(a)(b), it can be seen that the change rules of the C_y of the HC of TA and TB obtained from the three schemes are consistent, and the difference lies in the amplitude differences between the peaks and valleys of the C_y obtained from the three schemes. Specifically, the maximum differences between the C_y of the HC of TA and the HC of TB obtained by Scheme 2 and Scheme 3 are 2.36% and 2.52% at the peak and trough, respectively, while the maximum differences between the C_y of the HC of TA and the HC of TB obtained by Scheme 1 and Scheme 3 are 7.32% and 7.61% at the peak and trough, respectively. The C_y of the HC of TA and the HC of TB obtained by scheme 2 are closer to those of Scheme 3. Therefore, to save computational costs, the grid generation method of Scheme 2 is adopted.

3.2 Time Step Independence Verification

In addition to verifying the independence of the grid, it is also necessary to verify the opposition of the time step (Du et al., 2022). Therefore, based on the above grid independence verification, a time step independence verification is performed using the grid of Scheme 2. Three different time steps, 0.01 s, 0.001 s, and 0.0005 s, are selected for the time step independence verification. The number of iterations for each time step is chosen to be 30, as it is clearly observed that the residual curves reach convergence and level off by iterating 30 times within each time step. Figures 9(a)(b) show the C_y obtained for the HC of TA and TB for the three different

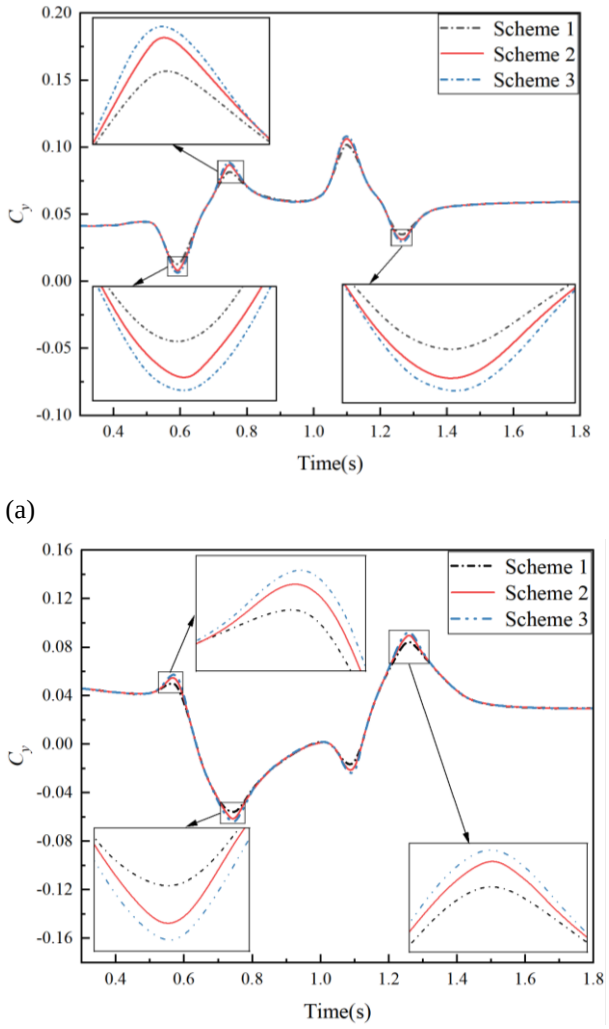

Fig. 8 Grid independence validation: (a) C_y of the HC of TA; (b) C_y of the HC of TB

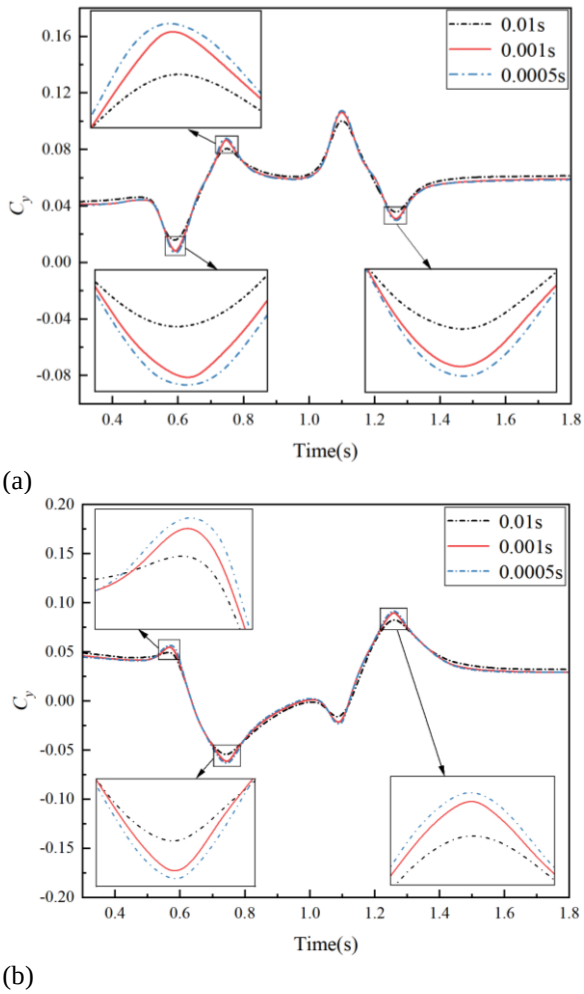

Fig. 9 Time independence verification: (a) C_y of the HC of TA; (b) C_y of the HC of TB

time steps. From the figure, it can be found that the C_y obtained for the HCs of trains A and B at a time step of 0.01 s are greatly different from those obtained at time steps of 0.001 s and 0.0005 s, while the C_y obtained for the HC s of trains A and B at a time step of 0.001 s are in good agreement with those obtained at a time step of 0.0005 s. Therefore, a time step of 0.001 s is reasonable and can be used for the following research.

3.3 Experimental Verification

To verify the accuracy of the turbulence model, overset grids, and boundary condition methods used in this study, the numerical simulations conducted in this study must be experimentally validated with a dynamic model. Therefore, the data obtained by Meng et al. (2021) dynamic modelling experiment are compared with the simulation results obtained in this study. The moving model experiment uses two 1:20 scale models of three-unit HSTs passing at 350 km/h (97.22 m/s). The train surface pressure at the monitoring point on the meeting side of the trains is selected to compare the pressure wave results of the dynamic model test and numerical simulation, as shown in Fig. 10. The change in the train surface pressure

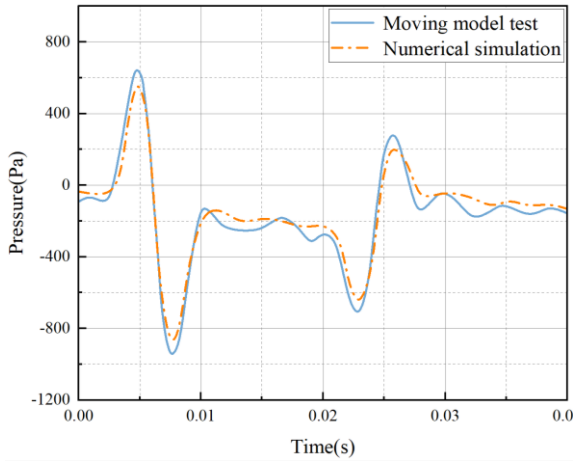

Fig. 10 Experimental verification of the dynamic model

obtained by the simulation is in good agreement with the results obtained by the dynamic model test. Although there are some differences, especially at the peak and trough of the pressure, between t = 0.01 s and t = 0.02 s and between t = 0.03 s and 0.04 s, the amplitude difference between the two is not more than 10%, and the deviation

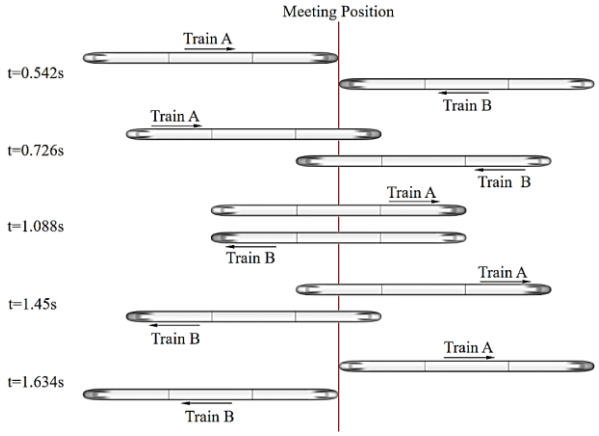

Fig. 11 Important relative positions and their moments during the intersection of HSTs

may be caused by the difference between the train models used in the experiment and the simulation. Therefore, we can conclude that the numerical method applied in this study is reasonable and reliable.

4. RESULTS AND DISCUSSION

Figure 11 shows the relative positions of the five important moments at which the HSTs meet on the bridge. The red vertical line in the figure is the intersection position of the HSTs. This section analyses the vortexes generated by the trains and the surface pressure distributions of the trains at these five moments.

4.1 Vortex Evolution

An important factor affecting the safe driving of trains is the formation, shedding, and dissipation of vortexes around the trains, and the vortexes around the trains will become more complex when the trains meet. Therefore, it is necessary to study the vortexes generated when trains meet. The IDDES method used in the study can simulate vortex structures at different scales, so the Q-criterion method is used to identify the vortex structures around the trains and the windshield wall. The Q-criterion has an equivalent surface value of 200, which is colored by the velocity.

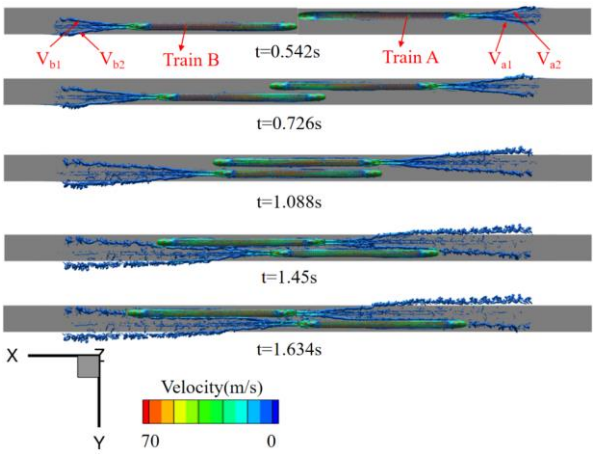

Fig. 12 Evolution process of the vortexes around the trains in Case 1

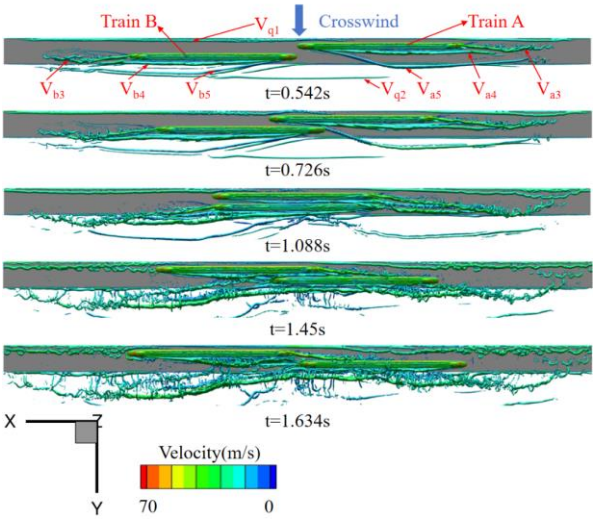

Fig. 13 Evolution process of the vortexes around the trains in Case 2

From Fig. 12, it can be observed that the flow separation of air occurs mainly in the TC, where a pair of vortexes Va1 and Va2 with opposite rotational directions are generated at the TC baffle. In addition, a pair of relatively small vortices are generated on both sides of the streamlined area of the TC, such as the vortex between Va1 and Va2 in Fig. 12. At the intersection of trains, the vortex continues to rotate to the rear of each train. As the energy of the vortex decreases during movement, the vortex structures gradually become larger. During movement, it gradually decomposes into a large number of small-scale vortex structures. These vortex structures evolve towards the rear and width of the train. After the two trains are parallel, vortex Vb1 intersects with TA, and vortex Va1 intersects with TB. As the trains run, the intersection area between the vortex and the train becomes increasingly larger, which increases the unsteady characteristics of the flow field around the train and affects the surface pressure distribution of the train, thus affecting the aerodynamic load of the train and ultimately affecting the safety of the train.

It can be seen from Fig. 13 that, compared with the situation without crosswind, the vortexes around the train change greatly when there is crosswind. Vortexes Va3 and Vb3 generated by the streamlined area of the two TCs no longer appear in pairs, but the windward side (WS) of the streamlined area generates one vortex alone and moves to the leeward side (LS). A vortex is also generated at the baffle and interacts with the vortex generated in the streamlined area. Due to the effect of crosswind, large-scale vortexes Va4 and Vb4 are generated at the junction of the LS and the top surfaces (TS) of the two HCs, respectively, forming a small-angle backwards movement with the trains. At the same time, large-scale vortexes Va5 and Vb5 are also generated at the baffle of the two HCs, and a large-angle backwards movement is formed with the trains. The WS and LS of the bridge deck also produce long strip-shaped vortexes Vq1 and Vq2, respectively. After the two trains intersect, vortexes Va4 and Va5 formed by TA intersect with TB; when the two trains are juxtaposed, vortexes Va4 and Va5 are truncated and move

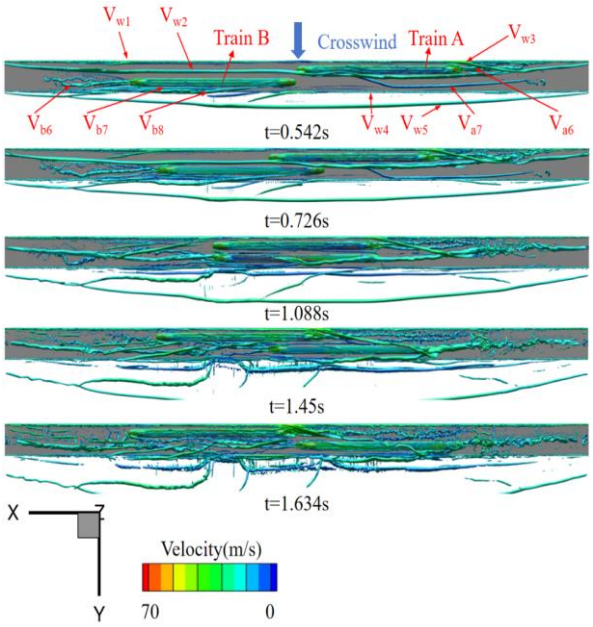

Fig. 14. Evolution process of the vortexes around the trains in Case 3

and decompose with the crosswind downstream. At the same time, vortexes Va4 and Va5 are constrained between the two trains. When the two trains end in parallel, the vortex Va3 generated by TA intersects with TB, and then Va3 is truncated, moving and decomposing with the crosswind. However, when the two trains are juxtaposed, the vortexes generated by TB do not intersect with TA. When the trains end in parallel, a part of vortex Vb3 generated by TB merges with vortexes Va4 and Va5 generated by TA. When the trains meet under crosswind, the vortex structure around the trains is very complex, and the stability of the trains is more threatened.

From Fig. 14, it can be noted that with the windbreaks, no more vortices are generated at the junction of the LS and the TS of the HC of TA; under the induction of the streamlined area of the TC of TA, a large-scale vortex Vw3 is generated at the upper end of the corresponding windbreaks, and the position of the vortex moves forward with TA. The two vortexes Vb7 and Vb8 generated by the LS of TB are confined in a narrow space between TB and the downstream windbreak. In addition to the vortex generated by the train, the windbreaks also generate other vortexes. Among them, very long, large-scale vortexes Vw2 and Vw5 are generated at the upper ends of the upstream and downstream windbreaks, respectively, and a large number of small vortexes Vw1 are generated on the square pore surface of the windbreaks. When the trains intersect, the vortex Vw2 intersects with the TS of the TA. It moves downstream with the crosswind, intersects with TB, and is cut into two parts. The contact part with the HC of TB is integrated with vortexes Vw3 and Va6, and the contact part with the TC of TB is integrated with Vb6. After the end of the train juxtaposition process, TB intersects with vortexes Vw3 and Va6, while TA almost does not intersect with Vb6. Under the action of the windbreaks, the vortexes generated by the two TCs do not follow the downstream movement of crosswind but rather expand, decompose, and dissipate on the bridge deck.

Through the above analysis, it can be seen that the crosswind has a significant impact on the vortex generated by each train, and the vortex generated by TA has a greater impact on TB during the train rendezvous, while the vortex generated by TB has a smaller impact on TA. In the presence of a windshield wall, TA is less affected by the crosswind than TB, and the aerodynamic load of TB is more complex than the aerodynamic load of TA. Therefore, when the trains meet under the action of crosswind, the safety and stability of TB are worthy of attention.

4.2 The Change in the Train Surface Pressure Distribution

The pressure distribution on the surface of a HST is another important factor affecting its aerodynamic performance (Zhou et al., 2023). As shown in Fig. 15(a), the pressure distribution at the nose tip of the TC is not as uniform as that at the nose tip of the HC because the vortex at the nose tip of the TC falls off from the surface of the train, which makes the flow field in this area chaotic. A strong NP area is formed in the area where the upper edge of the windshields of the HC and TC intersect, and the pressure of the two trains is symmetrically distributed in the transverse direction. As shown in Fig. 15 (b), when t = 0.726 s, a strong local positive pressure (PP) zone appears on the LS of TA and the WS of TB, which is due to the PP wave at the nose tips of the two train heads. As the train rendezvous proceeds, this PP zone appears on the corresponding surfaces of the two trains in sequence over time. The NP in the intersection area of the two trains increases, which is due to the obstruction of the air flow between the two trains in the intersection area, making the flow field more complicated. As shown in Fig. 15 (c), when t = 1.088, the two trains are juxtaposed. At this time, the intersection area of the two trains is maximized, and the NP on the intersection side increases again. As shown in Fig. 15 (d), when t = 1.45 s, the local strong PP zone on the LS of TA and the WS of TB is caused by the PP wave at the nose tip of TC of TB and the nose tip of TC of TA. As shown in Fig. 15 (e), when t = 1.634, the two trains end their rendezvous. From the analysis conducted in Section 4.1, it can be seen that the vortexes shedding from the TCs of TA and TB have certain influences on TB and TA, respectively, but these influences are small when there is no crosswind.

Comparing Figs. 15 and 16, it can be found that the surface pressure distribution of the train changes greatly when the two trains meet under the conditions of Case 1 and Case 2. Under the influence of crosswind, the PP areas at the nose tip of the HC, the junction of the windshield and the nose tip, and the baffle are all shifted to the WS, while the PP areas at the nose tip of the TC and the junction of the windshield and the nose tip are all shifted to the LS; the strong NP zone at the junction with the upper edge of the windshield of the HC shifts to the LS, and the strong NP zone at the junction with the upper edge of the windshield of the TC shifts to the WS. The pressure imposed on the WS of the train is greater than that on the LS; strong NP appears in the area where the WS of the train intersects with the TS, which is a typical feature caused by crosswind. Comparing the pressure

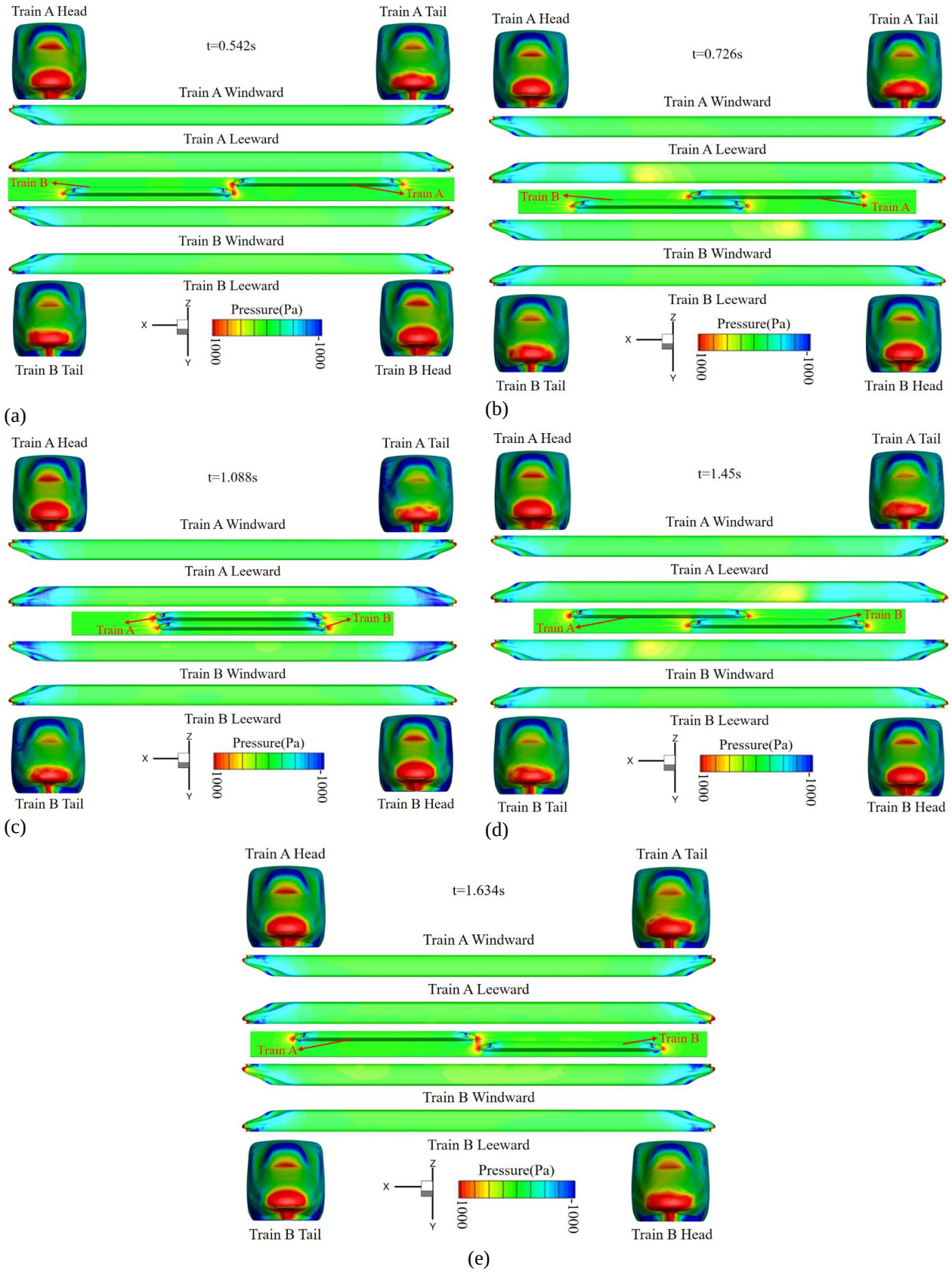

Fig. 15 Pressure distribution on the train surfaces under Case 1

distributions on the WS and LS of the train, it can be found that the pressure distribution on the WS is uniform, while the pressure distribution on the LS is messy, which is consistent with the conclusion drawn by Zhou et al. (2023). As shown in Fig. 16(b), at t = 0.726 s, a localized PP region is formed on the meeting surface of TA under the influence of the pressure wave at the nose tip of the HC of TB. The PP at the meeting surface of TB is reduced due to the blocking of crosswind by TA and the formation of vortices in the meeting gap formed between the two trains. Influenced by the NP in the streamlined area on the LS of the HC of TA, a localized NP area is formed on the

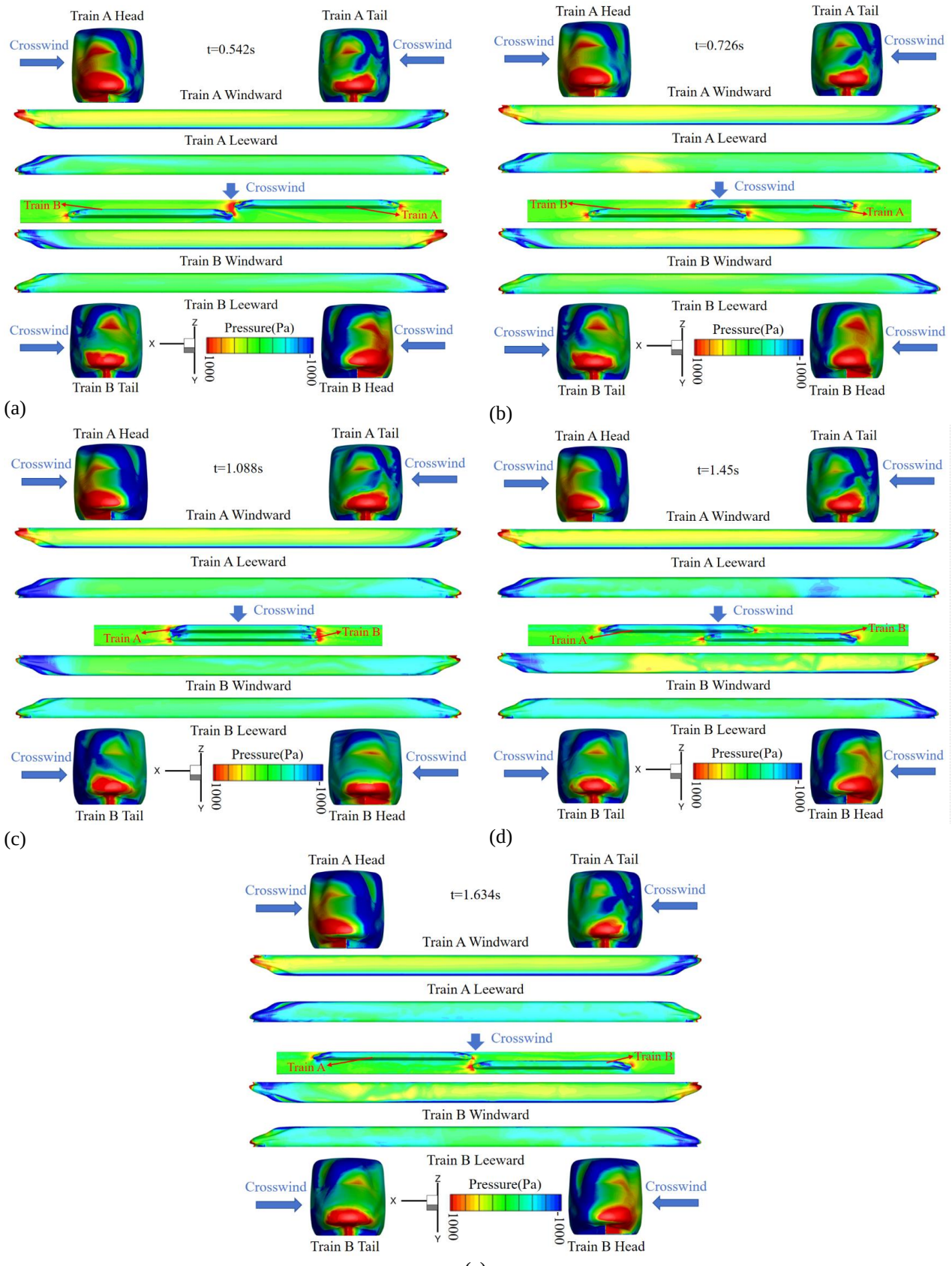

Fig. 16 Pressure distributions on the train surfaces under Case 2

WS of TB. As shown in Fig. 16 (c), when t = 1.088 s, the two trains are parallel, the pressure on the WS of TB changes from positive to negative, and the NP areas in the streamlined area on the LS of TA and the streamlined area on the WS of TB increase. This is because the streamlined parts of the HC and TC are complex, and the flow field and vortex in the gap between the two trains are more chaotic and complex than those in other areas. As shown

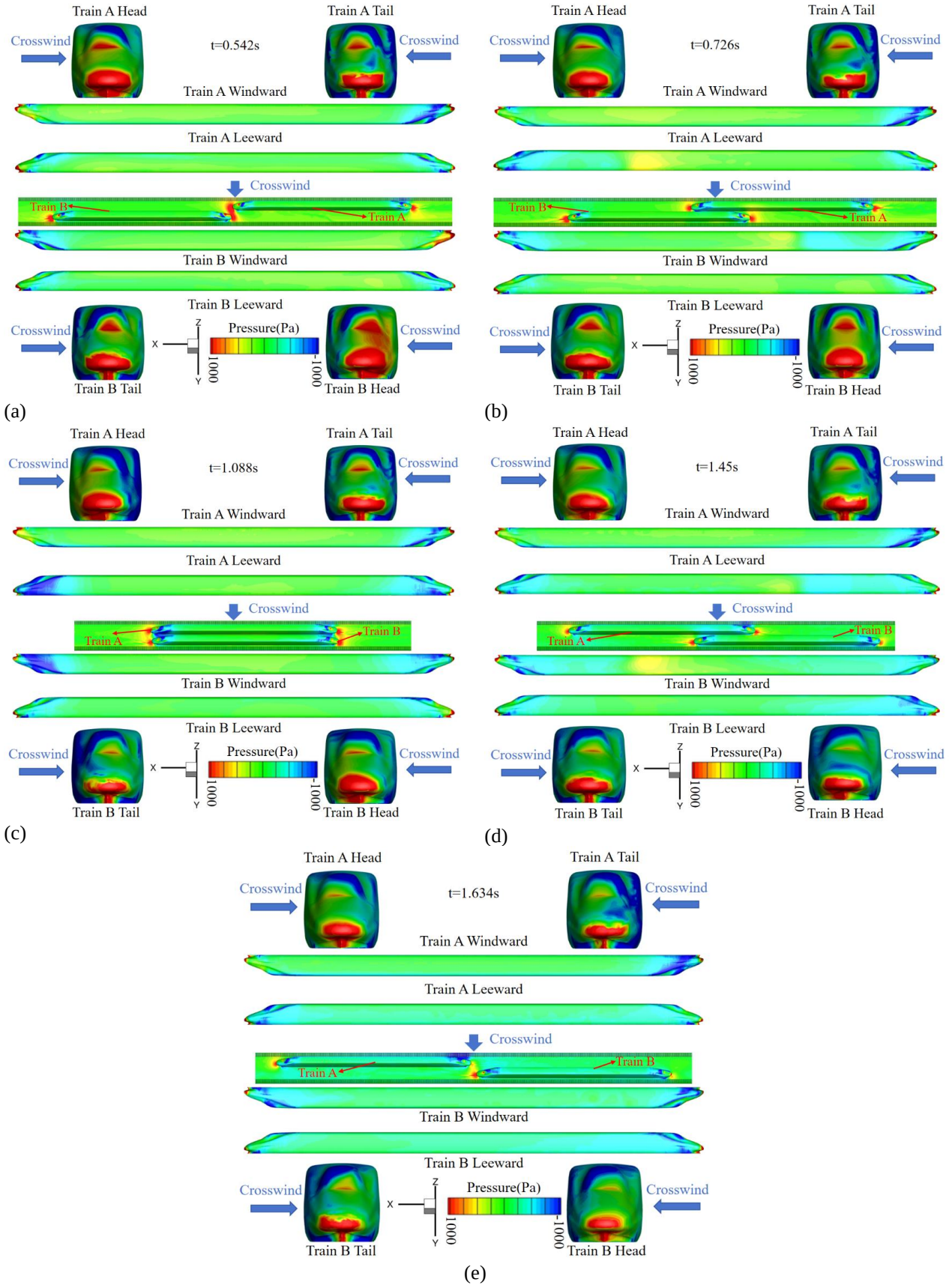

Fig. 17 Pressure distribution imposed on the train surfaces under Case 3

in Fig. 16(d), the trains end the parallel state at t = 1.45 s because the WS of the nose tip of the TC of TB is NP, so a strong local NP zone is formed on the LS of TA. Because the LS of the nose tip of the TC of TA is PP, a local PP zone is formed on the WS of TB. As shown in Fig. 16 (e), when t = 1.634 s, the two trains no longer intersect. From the analysis conducted in Section 4.1, it can be seen that the vortex generated by TB has little effect on TA, while

the vortex generated by TA has a certain effect on TB, which makes the pressure distribution on the WS of TB sharply unstable.

Figure 17 is the pressure cloud map of the train surfaces when the HSTs meet under the condition of Case 3. Compared with the pressure cloud map of the train surfaces under the condition of Case 2, the windbreaks obviously improve the pressure distribution of the train surfaces, and the NP imposed on the train surfaces are obviously reduced; thus, the pressure distribution of the train surfaces is more similar to that without crosswind. For example, as shown in Fig. 17 (d), at t = 1.45 s, the local high pressure formed on the LS of TA is PP, which is the same as that without crosswind. The following contents quantitatively study the pressure changes imposed on the train surfaces in these three cases.

To quantitatively compare the surface pressures imposed on the trains when they meet in three cases, the trains at the end of the meeting are selected as the research objects, and the pressure curves on the WS, LS, TS, and cross sections of the HCs of TA and TB are analyzed. Figure 18 shows the surface pressure curve of TA. From Fig. 18(a), it can be found that the WS of TA experiences PP under Case 2, and the surface pressure fluctuation of the body is very small; in Case 3, due to the effect of the windbreaks, a backflow is formed between the train and the windbreaks, and the flow field in this area is disordered. Therefore, the pressure on the WS of the train is negative, and the pressure fluctuation is large. A strong NP area is formed in the streamlined area of the TC, which is mutually verified with the analysis of the pressure cloud map on the surface of the train. From Fig. 18(b), it can be seen that the pressure fluctuation on the LS of TA is larger than that on the WS in the three cases. The analysis conducted on the vortices generated by the trains in Section 4.1 shows that the pressure fluctuations on the train surfaces in Case 2 and Case 3 are due to the vortices formed by TA on the LS, whereas the fluctuation on the train surfaces in Case 1 is due to the vortices generated by TB that intersect with TA. As shown in Fig. 18(c), the pressure on the TS of each train is close to zero when there is no crosswind, and the TS of each train experiences NP under Case 2 and Case 3. In Figs. 18 (d) and 19 (d), BS is the bottom surface. Under Case 2, the area at the junction of the WS and the TS of TA (the light blue area in the figure) forms a strong NP field (approximately -1400 Pa), and the NP formed in this area under Case 3 is relatively small (approximately -520 Pa). The NP imposed under Case 3 is 62.8% lower than that under Case 2. For TB, the NP formed in this area under Case 2 is approximately -1120 Pa, and the NP formed in this area under Case 3 is approximately 400 Pa. Compared with that in Case 2, the NP formed in Case 3 is reduced by 64.2%. Therefore, it is shown that the windbreaks can reduce the NP imposed on the surfaces of the trains when the trains are running under crosswind, improve the pressure distribution on the surfaces of the trains, and improve the driving safety of the trains. Figure 19 shows the curve of the change exhibited by the train surface pressure of TB. As a whole, the train surface pressure change shown by TB is relatively close to that of TA. The difference is that TB is affected by the vortex generated by TA, and the pressure fluctuation observed on the train surface is larger, as shown in Figs. 19 (a), (b), and (c).

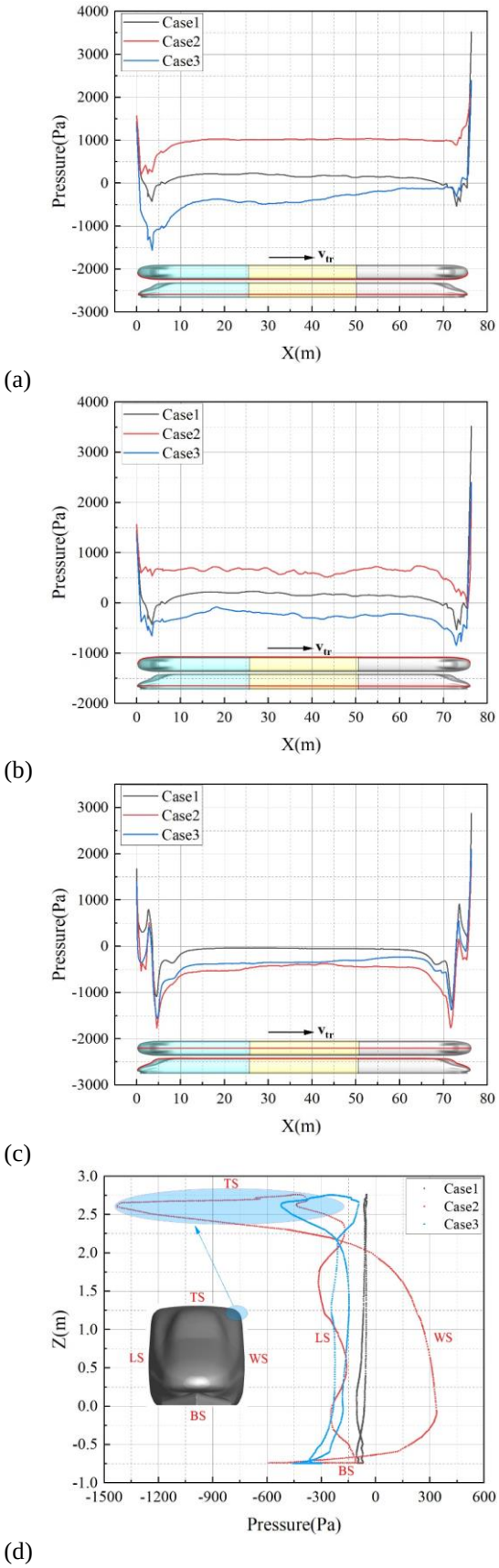

Fig. 18 Surface pressure curves of TA at t=1.088 s: (a) WS; (b) LS; (c) TS; (d) HC section

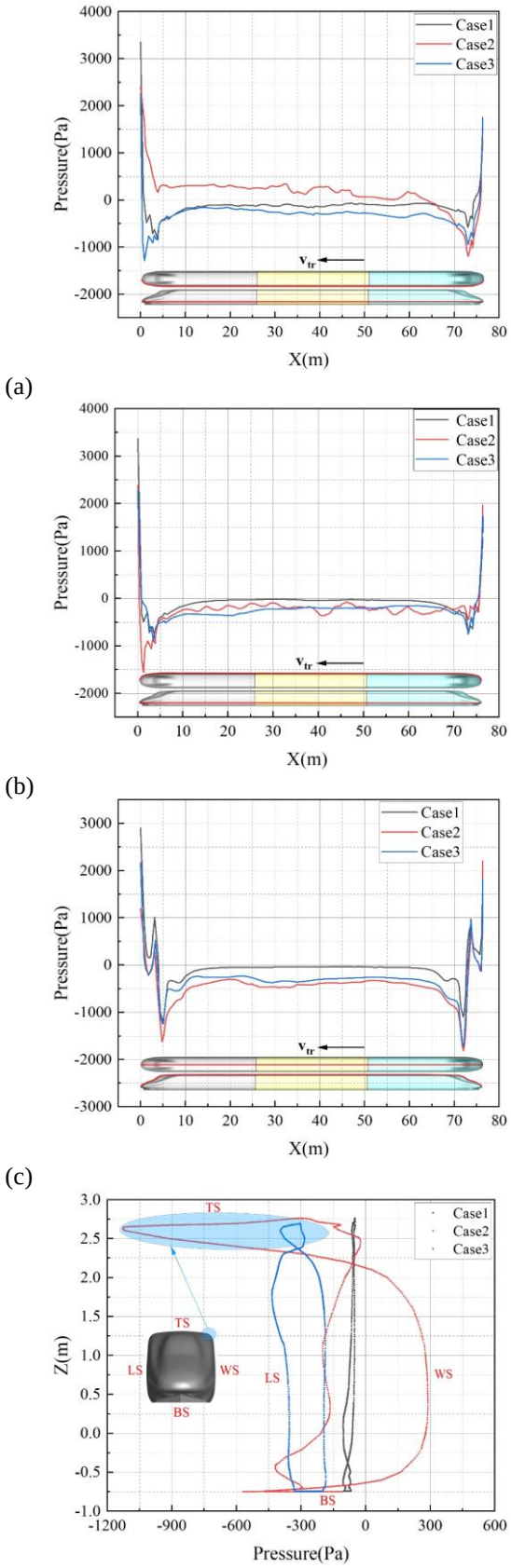

Fig. 19 Surface pressure curves of TB at t=1.088 s: (a) WS; (b) LS; (c) TS; (d) HC section

Although the windbreaks can improve the pressure distribution on the surface of a train and improve the safety of the train, the pressure wave generated by the train also has a pneumatic impact on the windbreaks, affecting the installation stability of the windbreaks and thus affecting the safety of the train. When the train enters the rendezvous, the air around the nose of the HC is rapidly squeezed, forming a PP wave near the nose of the HC that first compresses and then expands. This pressure wave spreads to the windbreaks, forming a PP area in the windbreaks, and the PP area of the upstream windbreaks is larger than that of the downstream windbreaks, as shown in Fig. 20. The NP wave formed in the streamlined area on the WS of the TC of TA spreads to the LS of the windbreaks, forming NP areas on the WS of the windbreaks; this is consistent with the results of the Xiang et al. (2015) analysis. The PP exerted by the nose tip of the TC has little effect on the windbreaks. Overall, the impact of TA on the upstream windbreaks is greater than that of TB on the downstream windbreaks because the PP region generated at the nose tip of the HC of the TB is biased towards the WS, whereas the PP region generated at the nose tip region of the TC is smaller than the PP region that grows at the nose tip region of the HC.

4.3 Aerodynamic Load Coefficients of Trains

When HSTs meet under crosswind, the flow field around the trains changes continuously as the trains pass each other. The F_z, F_y and M_x of the trains are more prominent than other aerodynamic forces. Therefore, this study analyses the time-dependent curves of the C_z, C_y and C_{mx} of the HC, MC and TC during the intersection process under three working conditions.

It can be seen from Fig. 21 and Fig. 22 that the F_z directions of TA and TB are the same during the whole train intersection process, while the directions of the F_y and M_x are opposite. In Case 1, the values of the aerodynamic load coefficients of the two trains are equal; before the intersection of the trains, except when the C_z of the HC is less than 0, the aerodynamic load coefficients of the HC, MC and TC of each train are close to 0; the C_z and C_y of each train are larger than the C_{mx}; and the C_z, C_y and C_{mx} all exhibit two significant sudden changes, which are due to the formation of the rendezvous pressure wave, as shown by the analysis of the train surface pressure in Section 4.2. In Case 2, the aerodynamic load coefficients are no longer equal to 0 before the meeting of the two trains; during the train meeting process, due to the combined effect of crosswind and the train wind, the aerodynamic load coefficients of the trains are obviously greatly different, the values of the corresponding aerodynamic load coefficients of TA and TB are no longer equal, and the aerodynamic load coefficients of TB are more unstable. The two mutations of the C_{mx} of the MC of TA, the C_z of the TC of TA, the C_z of the MC and the TC of TB, and the C_{mx} of the HC of TB are no longer obvious. In Case 3, due to the effect of the windbreaks, the aerodynamic load coefficients of the two trains are significantly reduced, the two mutations are more obvious than those observed without the windbreaks, and the change trend is closer to that without crosswind. Therefore, the windbreaks can reduce the aerodynamic load of the trains during their intersection and improve the safety of the trains. From Figs. 21 (h) (i) and Figs. 22 (h) (i), it can be found that the C_y and C_{mx} of the TC in Case 2 and Case 3 are negative before the intersection, and the

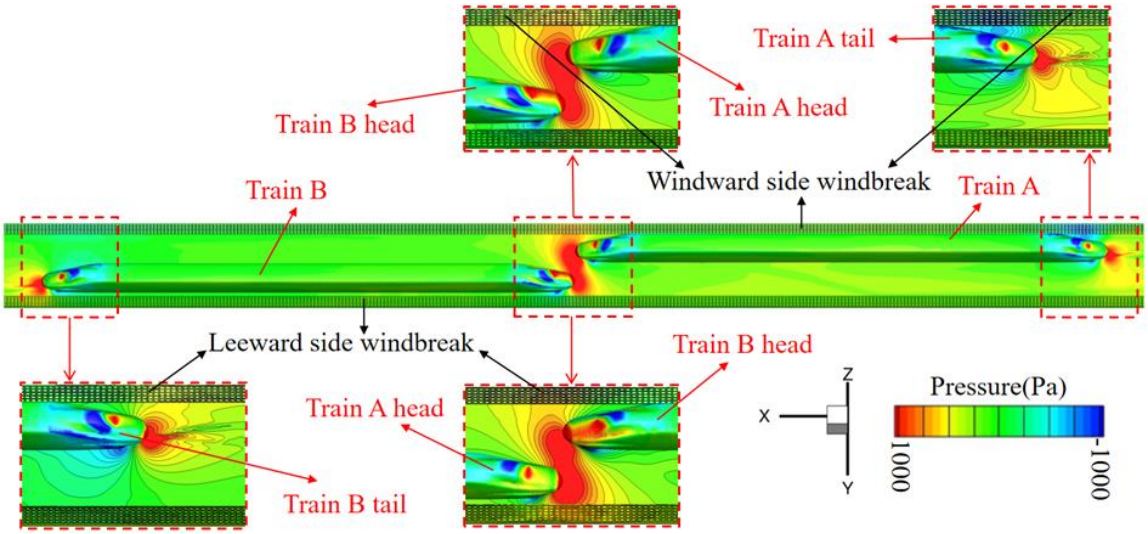

Fig.20 Effect of pressure waves on windbreaks

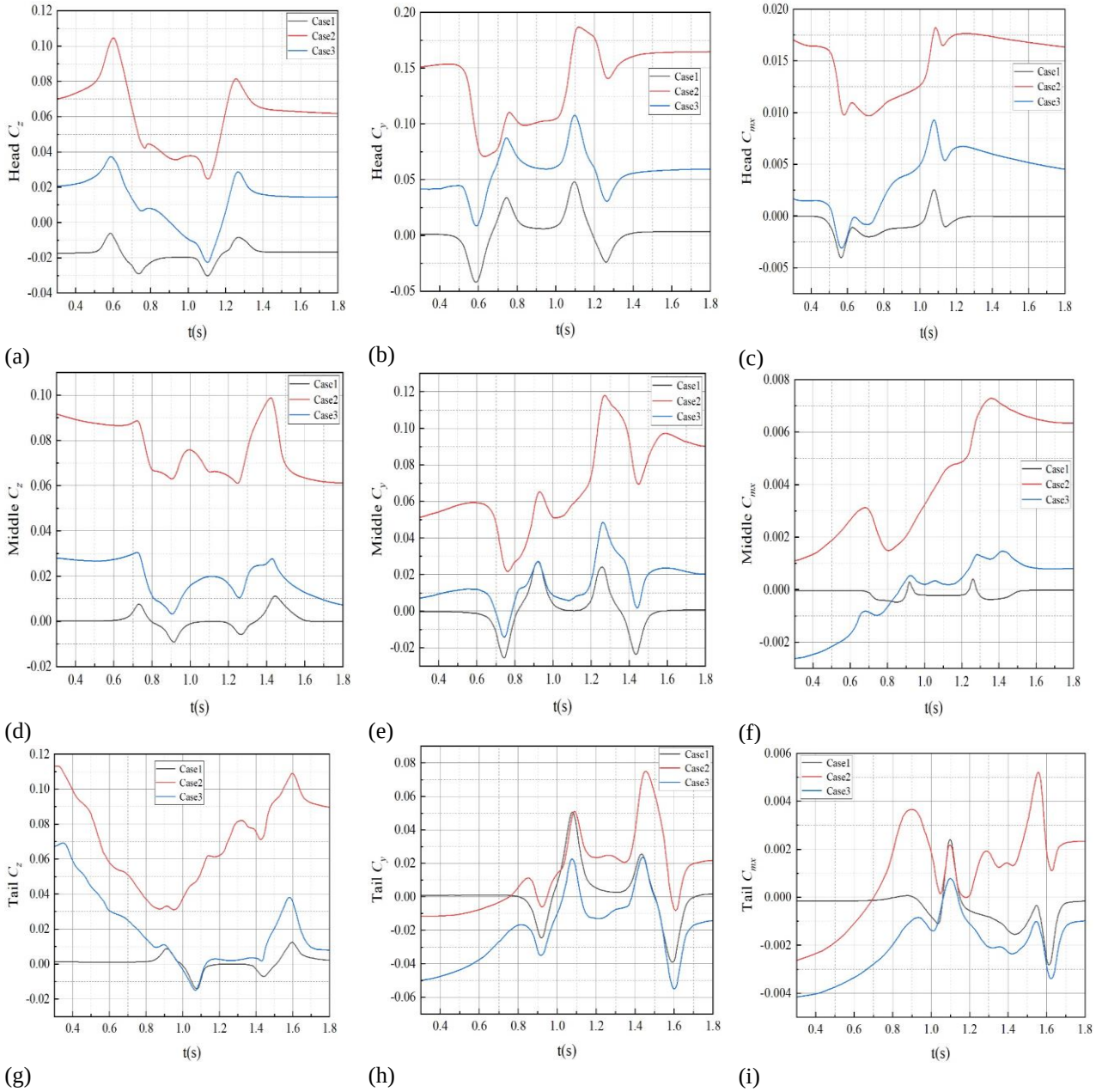

Fig. 21 Aerodynamic load coefficients of the HC, MC and TC of TA

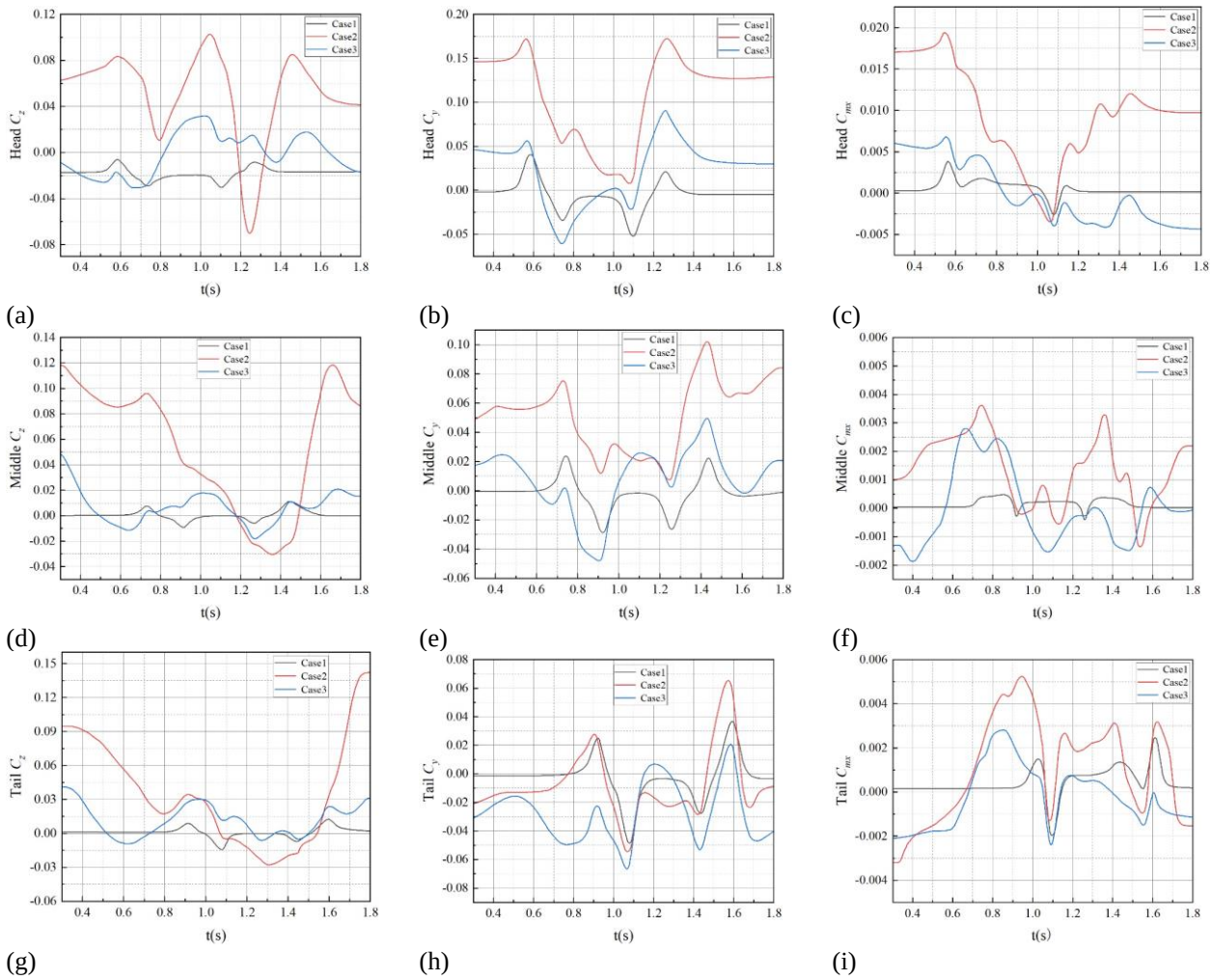

Fig. 22 Aerodynamic load coefficients of the HC, MC and TC of TB

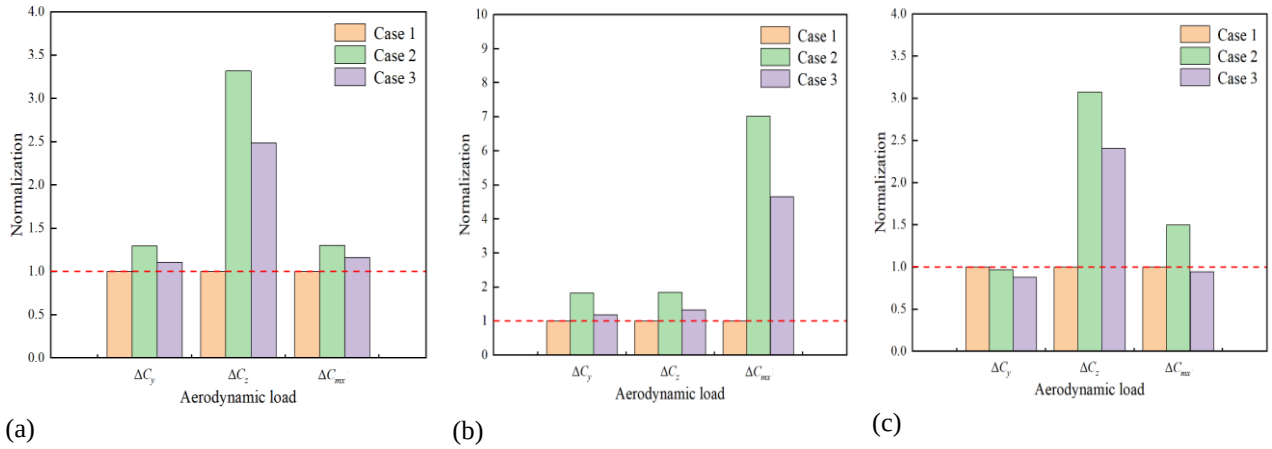

Fig. 23 Normalization of the aerodynamic load of TA: (a) HC; (b) MC; (c) TC

values in Case 3 are larger. From the analysis of the surface pressure distribution of the trains in Section 4.2, it can be known that due to the influence of crosswind, strong NP is formed in the streamlined area on the WS of the TC of the train. By comparing Figs. 21 and 22, it can be seen that the aerodynamic load of TB is more unstable than that of TA. When the two trains meet under crosswind, a greater safety hazard is induced when TB is driving. It is necessary to pay more attention to the driving safety of TB.

Figures. 23 and 24 are the normalized diagrams of the amplitudes of the aerodynamic loads of the HC, MC and TC of TA and TB. To quantitatively analysis the protective performance of the windbreaks for HSTs, the load coefficient amplitude (ΔC) is defined as follows (Ouyang. et al., 2023):

$$\Delta C = C_{max} - C_{min} \tag{6}$$

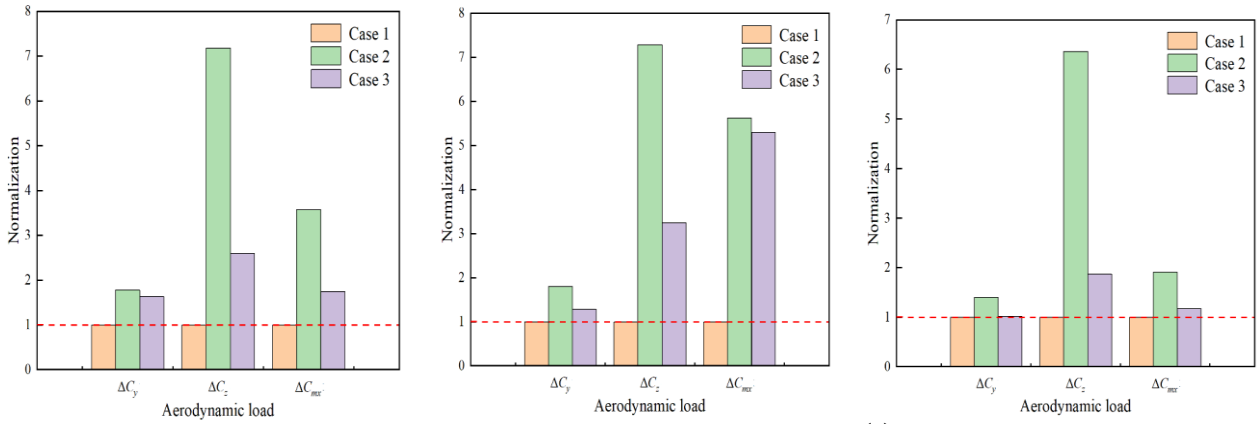

Fig. 24 Normalization of the aerodynamic load of TB: (a) HC; (b) MC; (c) TC

where ΔC represents the amplitude of the load coefficient and C_{max} and C_{min} represent the positive and negative peak coefficients, respectively.

As seen in Fig. 23, the C_y, C_z, and C_{mx} of the HC of TA in Case 1 increase by 29.5% (18.9%), 231.8% (148.9%), and 30% (16.3%), respectively, over those of TA for Case 2 (Case 3); the C_y, C_z and C_{mx} of the MC of TA increase by 82.3% (18.8%), 84.8% (33.4%) and 602.2% (365.1%), respectively; the C_y, C_z and C_{mx} of TC of TA increased by -3.3% (-12.2%), 207.4% (140.7%) and 49.9% (-5.6%), respectively. Compared with the aerodynamic load coefficients of TA in Case 2, the C_y, C_z and C_{mx} of the HC of TA in Case 3 are reduced by 14.7%, 25% and 10.6%, respectively; the C_y, C_z and C_{mx} of the MC of TA are reduced by 34.9%, 27.8% and 33.8%, respectively; and the C_y, C_z and C_{mx} of the TC of TA are reduced by 9.2%, 21.7% and 37%, respectively.

As shown in Fig. 23, the C_y, C_z, and C_{mx} of the HC of TB in Case 1 increase by 77.7% (63.4%), 618.5% (159.7%), and 258% (74.5%), respectively, over those of TB for Case 2 (Case 3); the C_y, C_z and C_{mx} of the MC of TB increase by 80.6% (28.8%), 628.6% (225%) and 462.6% (429.8%), respectively; and the C_y, C_z and C_{mx} of the TC of TB increase by 40.3% (2.3%), 536.7% (87.7%) and 91.2% (17.9%), respectively. Compared with the aerodynamic load coefficients of TB in Case 2, the C_y, C_z and C_{mx} of the HC of TB in Case 3 are reduced by 8%, 63.9% and 51.3%, respectively; the C_y, C_z and C_{mx} of the MC of TB are reduced by 28.7%, 55.3% and 5.8%, respectively; and the C_y, C_z and C_{mx} of the TC of TB are reduced by 27.1%, 70.5% and 38.3%, respectively.

The coefficients of the F_y imposed on the TC of TA in Case 2 and Case 3 are smaller than those in Case 1 because of the strong NP region in the streamlined area on the WS of the TC, which is larger when there are windbreaks. From Figs. 23 and 24, it can be seen that the effect of crosswind on the F_z of the HC, MC and TC of TB is greater than that for TA because TB is located downstream and away from the windbreaks on the WS. From the above data analysis, it can be concluded that when HSTs meet on a bridge under the action of crosswind, the windbreaks can effectively reduce the F_y, F_z and M_x of HC, MC and TC and greatly improve the safety of the train intersection.

5. CONCLUSION

(1) Under the action of crosswind, the vortexes generated by the trains are no longer symmetrical, and two large vortices are formed on the LS of the trains, which move downstream along the crosswind at a certain angle with the trains. When there are windbreaks, no vortex is generated in the streamlined area on the LS of TA; a vortex is generated at the upper end of the upstream windbreak to intersect TA and TB in turn; the vortex generated by the two TCs does not follow the crosswind downstream but is instead expanded, decomposed, and dissipated on the bridge deck.

(2) When there is no crosswind, the surface pressure of the trains is symmetrically distributed in the lateral direction. When there is a crosswind, the PP area at the nose tip of the HC is shifted to the WS, while the NP area at the upper edge of the windshield is shifted to the LS, and the pressure distribution of the TC is the opposite of that of the HC; a NP area is formed on the WS of the trains at the junction area of the WS and the TS; when there are windbreaks, the pressure imposed on the train surfaces decreases. During the meeting process of the trains, the pressure waves generated at the nose tips of the HC and the TC form a high-pressure region on the LS of TA and the WS of TB in turn.

(3) When trains are at an intersection, a PP wave that first compresses and then expands near the nose tip of the HC forms a PP area on the windbreaks. The PP area of the upstream windbreaks is larger than that of the downstream windbreaks. The NP wave of the upstream windbreaks formed by the streamlined area on the WS of the TC of TA forms a NP area. The PP wave generated by the nose tip area of the TC of the TB forms a PP area on the downstream windbreaks. These pressure waves affect the installation stability of the windbreaks, thus affecting the safety of the train.

(4) When there is no crosswind, the C_z, C_y and C_{mx} of the trains exhibit two sudden changes during the intersection process, and the C_z, C_y and C_{mx} of TA and

TB are equal. When there is a crosswind, the C_z, C_y and C_{mx} of the two trains increase significantly; the windbreaks significantly reduce the C_z, C_y and C_{mx} of the trains when they meet under crosswind. The C_z, C_y and C_{mx} of TB are more unstable than those of TA, and more attention should be given to the driving safety of TB.

ACKNOWLEDGEMENTS

Thanks to the National Natural Science Foundation of China (51968069) for the support of this study.

CONFLICT OF INTEREST

The author(s) declared no potential conflicts of interest with respect to the research, authorship, and/or publication of this article.

AUTHORS CONTRIBUTION

L. X. Chen: Formal analysis, Validation, Writing - original draft; **A. F. Jin**: supervision; review and editing; contributed to answering comments; **X. C. Jia**: Resources, Supervision.

REFERENCES

Cai, L., Lou, Z., Li, T., & Zhang, J. (2020). Numerical study on the effects of anti-snow deflector on the wind-snow flow underneath a high-speed train. *Journal of Applied Fluid Mechanics, 14*(1), 287-299. https://doi.org/10.47176/jafm.14.01.31375

Deng, E., Yang, W. C., He, X. H., Ye, Y. C., Zhu, Z. H. & Wang, A. (2020). Transient aerodynamic performance of high-speed trains when passing through an infrastructure consisting of tunnel–bridge–tunnel under crosswind. *Tunnelling and Underground Space Technology*, *102*, 103440. https://doi.org/10.1016/j.tust.2020.103440

Deng, E., Yang, W. C., He, X. H., Zhu, Z., Wang, H. F., Wang, Y. W., Wang, A., & Zhou, L. (2021). Aerodynamic response of high-speed trains under crosswind in a bridge-tunnel section with or without a wind barrier. *Journal of Wind Engineering and Industrial* Aerodynamics, 210, 104502. https://doi.org/10.1016/j.jweia.2020.104502

Du, L. M., Bian, C. J., & Zhang, P. (2022). Aerodynamic response analysis of high-speed trains passing through high platforms under crosswind. *Journal of Applied Fluid Mechanics*, *15*(5), 1525-1543. https://doi.org/10.47176/jafm.15.05.1045

He, Y. W. (2017). Design of the wind-resistant gallery in Lanzhou-Xinjiang high speed railway. *Journal of Railway Engineering Society*, *6*, 55–9. https://doi.org/10.3969/j.issn.1006-2106.2017.06.011.

Ji, P., Feng, Z. L., & Liao, S. L. (2022). Pedigree aerodynamic shape design of high-speed trains. *Journal of Applied Fluid Mechanics*, *16*(1), 193-204. https://doi.org/10.47176/jafm.16.01.1331

Li, M., Liu, B., Liu, T. H., & Guo, Z. J. (2020). Improved delayed detached eddy simulation of the slipstream and trackside pressure of trains with different horizontal profiles. *Journal of Applied Fluid Mechanics*, *13*(2), 457-468. https://doi.org/10.29252/jafm.13.02.30291

Li, W. H., Liu, T. H., Zhang, J., Chen, Z. W., Chen, X. D., & Xie, T. Z. (2017). Aerodynamic Study of Two Opposing Moving Trains in a Tunnel Based on Different Nose Contours. Journal of Applied Fluid Mechanics, 10(5), 1375-1386.doi: 10.18869/acadpub.jafm.73.242.27738

Li, Y., Wei, D. H., Qin, D., Yang, Y. H., & Li, T. (2021). Research on the pressure wave characteristics of high-speed trains passing each other at speeds of 400 km /h and above. *Journal of Railway Engineering Society*, (08), 25-29+35. https://doi.org/10.3969/j.issn.1006-2106.2021.08.006

Li, Y. L., Yang, Y., Wu, M. X., & Qiang, S. Z. (2015). Aerodynamic characteristics in the process of two trains passing each other on bridge under cross wind action. *China Railway Science*, (02), 37-44. https://doi.org/10.3969/j.issn.1001-4632.2015.02.06.

Liang, H., Sun, Y., Li, T., & Zhang, J. (2022). Influence of marshalling length on aerodynamic characteristics of urban emus under crosswind. *Journal of Applied Fluid Mechanics*, *16*(1), 9-20. https://doi.org/10.47176/jafm.16.01.1338

Lin, J., Kai, L., & Ming, R. (2019). The transient response of car body and side windows for high-speed trains passing by each other in a tunnel. *Composites Part B: Engineering*, *166*, 284-297, https://doi.org/10.1016/j.compositesb.2018.11.144

Liu, F., Yao, S., Zhang, J., & Zhang, N. (2016). Aerodynamic effect of EMU passing by each other under crosswind. *Journal of Central South University of Science and Technology*, (01), 307-313. https://doi.org/10.3969/j.issn.1672-7029.2016.06.004.

Mei, Y. G., Li, M. H., & Guo, R. (2019). Aerodynamic load distribution characteristics of pressure wave when trains passing each other in high-speed railway tunnel. *China Railway Science*, (06), 60-67. https://doi.org/CNKI:SUN:ZGTK.0.2019-06-009

Meng, S., Meng, S., Wu, F., Li, X. L., & Zhou, D. (2021). Comparative analysis of the slipstream of different nose lengths on two trains passing each other. *Journal of Wind Engineering and Industrial Aerodynamics*, *208*, 2021,104457. https://doi.org/10.1016/j.jweia.2020.104457

Niu, J. Q., Zhang, Y. C., Li, R., Chen, Z. W., Yao, H. D., & Wang, Y. (2022). Aerodynamic simulation of effects of one- and two-side windbreak walls on a moving train running on a double track railway line

subjected to strong crosswind. *Journal of Wind Engineering and Industrial Aerodynamics*, *221*, https://doi.org/10.1016/j.jweia.2022.104912

Ouyang, D. H., Deng, E., Yang, W. C., Ni, Y. Q., Chen, Z. W. , & Zhu, Z. H. (2023). Nonlinear aerodynamic loads and dynamic responses of high-speed trains passing each other in the tunnel–embankment section under crosswind. *Nonlinear Dynamics 111*, 11989–12015. https://doi.org/10.1007/s11071-023-08479-7

Qiao, Y. J., He, D. H., Chen, H. C., & Zhang, C. (2016). Study on influence of line spacing of high speed railway on pressure wave due to meeting of two oncoming trains. *High Speed Railway Technology*, (06),7-11+18. https://doi.org/10.3969/j.issn.1674-8247.2016.06.002.

Shur, M. L., Spalart, P. R., Strelets, M. K., & Travin, A. K. (2008). A hybrid RANS-LES approach with delayed-DES and wall-modelled LES capabilities. *International Journal of Heat and Fluid Flow*, *29*(6), 1638-1649. https://doi.org/10.1016/j.ijheatfluidflow.2008.07.001

Wang, M., Wang, Z. X., Qiu, X. W., Li, X. X., & Li, X. Z. (2022). Windproof performance of wind barrier on the aerodynamic characteristics of high-speed train running on a simple supported bridge. *Journal of Wind Engineering and Industrial Aerodynamics*, *223*, 104950. https://doi.org/10.1016/j.jweia.2022.104950

Wu, Z., Zhou, D., Li, S., Yang, J., Chen, G., & Li, X. (2022). Numerical analysis of the effect of streamlined nose length on slipstream of high-speed train passing through a tunnel. *Journal of Applied Fluid Mechanics*, *15*(6), 1933-1945. https://doi.org/10.47176/jafm.15.06.1189

Xi, Y. H., Mao, J., Liu, R. D., & Yang, G. W. (2016). Study on pressure wave amplitude of high-speed train meeting on open line. *Journal of South China University of Technology (Natural Science Edition)*, (03), 118-127. https://doi.org/10.3969/j.issn.1000-565X.2016.03.017.

Xia, Y. T., Liu, T. H., Su, X. C., Jiang, Z. H., Chen, Z. W., & Guo, Z. J. (2022). Aerodynamic influences of typical windbreak wall types on a high-speed train under crosswind. *Journal of Wind Engineering and Industrial Aerodynamics*, https://doi.org/10.1016/j.jweia.2022.105203

Xiang, H. Y., Li, Y. L., Wang, B., & Liao, H. L. (2015). Numerical simulation of the protective effect of railway wind barriers under crosswind. *International Journal of Rail Transportation.* http://dx.doi.org/10.1080/23248378.2015.1054906

Xu, G., Li, H., Zhang, J., & Liang, X. (2019). Effect of two bogie cavity configurations on the underbody flow and near wake structures of a high-speed train. *Journal of Applied Fluid Mechanics*, *12*(6), 1945-1955. https://doi.org/10.29252/jafm.12.06.29938

Xu, J. L., Sun, J. C., Mei, Y. G., & Wang, R. L. (2016). Numerical simulation on crossing pressure wave characteristics of two high-speed trains in tunnel. *Journal of Vibration and Shock*, (03),184-191. https://doi:10.13465/j.cnki.jvs.2016.03.029

Xu, R. Z., Wu, F., Su, W. H., Ding, J. F., & Vainchtein, D. (2020). A numerical approach for simulating a high-speed train passing through a tornado-like vortex. *Journal of Applied Fluid Mechanics*, *13*(5), 1635-1648. https://doi.org/10.36884/jafm.13.05.31080

Yang, W. C., Deng, E., He, X. H., Luo, L. S., Zhu, Z. H., Wang, Y. W. & Li, Z. T. (2021). Influence of wind barrier on the transient aerodynamic performance of high-speed trains under crosswinds at tunnel–bridge sections. *Engineering Applications of Computational Fluid Mechanics*, *15*(1), 727-746, https://doi.org/10.1080/19942060.2021.1918257

Yao, Y., Sun, Z., Li, G., Prapamonthon, P., Cheng, G., & Yang, G. (2022). Numerical investigation on aerodynamic drag and noise of pantographs with modified structures. *Journal of Applied Fluid Mechanics*, *15*(2), 617-631. https://doi.org/10.47176/jafm.15.02.32849

Zhang, J., Gao, G., Liu, T., & Li, Z. (2017a). Shape optimization of a kind of earth embankment type windbreak wall along the lanzhou-xinjiang railway. *Journal of Applied Fluid Mechanics*, *10*(4), 1189-1200. https://doi.org/10.18869/acadpub.jafm.73.241.27353

Zhang, J., He, K., Wang, J., Liu, T., Liang, X., & Gao, G. (2019). Numerical simulation of flow around a high-speed train subjected to Different Windbreak Walls and Yaw Angles. *Journal of Applied Fluid Mechanics*, *12*(4), 1137-1149. https://doi:.org/10.29252/jafm.12.04.29484

Zhang, J., He, K., Xiong, X., Wang, J., & Gao, G. (2017b). Numerical simulation with a des approach for a high-speed train subjected to the crosswind. *Journal of Applied Fluid Mechanics*, *10*(5), 1329-1342. https://doi.org/10.18869/acadpub.jafm.73.242.27566

Zhou, D., Xia, C. J., Wu, L. L., & Meng, S. (2023). Effect of the wind speed on aerodynamic behaviours during the acceleration of a high-speed train under crosswind. *Journal of Wind Engineering and Industrial Aerodynamics. Volume 232*, 105287. https://doi.org/10.1016/j.jweia.2022.105287